Effect of Long Waves on Ku-Band Ocean Radar Backscatter at Low Incidence Angles Using TRMM and Altimeter Data

Ngan Tran, B. Chapron, and D. Vandemark

***Abstract*—This letter uses a large ocean satellite data set to document relationships between Ku-band radar backscatter (σ_0) of the sea surface, near-surface wind speed (U), and ocean wave height (SWH). The observations come from satellite crossovers of the Tropical Rainfall Mapping Mission (TRMM) precipitation radar (PR) and two satellite altimeters, namely: 1) Jason-1 and 2) Environmental Satellite. At these nodes, we obtain TRMM clear-air normalized radar cross-section data along with coincident altimeter-derived significant wave height. Wind speed estimates come from the European Centre for Medium-Range Weather Forecast. TRMM PR is the first satellite to measure low incidence Ku-band ocean backscatter at a continuum of incidence angles from 0° to 18°. This letter utilizes these global ocean data to assess hypotheses developed in past theoretical and field studies—namely that variations in ocean sea state are measurably and systematically related to Ku-band σ_0, that the impact changes with incidence angle, and that it will affect the retrieval of wind speed from σ_0. Results have bearing on near-nadir ocean radar missions such as Surface Waves Investigation and Monitoring from Satellite, Advanced Scatterometer, TRMM, and the wide-swath altimeter.**

AQ1 ***Index Terms*—Author, please supply your own keywords or send a blank e-mail to keywords@ieee.org to receive a list of suggested keywords.**

I. Introduction

SATELLITE radars are used to infer the wind speed just above the sea surface through their measurement of backscattered signal power, which is a signal that changes with the amount and steepness of ocean waves. This normalized radar backscatter cross-section (σ_0) term also depends on the frequency, polarization, and incidence angle (θ) of the incident radiation. Two now-standard satellite systems for ocean wind estimation are the altimeter and the scatterometer. The former views the sea from a downlooking ($\theta = 0°$) incidence angle, whereas the latter uses side-looking angles from 20° to 60°. It is widely held that centimeter-scale ocean gravity-capillary waves and their growth or decay with wind forcing are the dominant controls of σ_0 variation for both sensors, but the ocean reflection is distinctly different for these two systems that is consistent with the optical expectation; increased wave roughness decreases altimeter σ_0 but increases it for the scatterometer. This is because the incidence angle leads to differing scattering processes: dominant quasi-specular scattering for the former and Bragg resonance diffraction for the latter. Regardless of such differences, the linkage between σ_0 and wind forcing is used for both sensors to empirically derive wind speed inversion algorithms that are well validated and widely used. However, long-wavelength tilting of short-scale waves is a known effect inducing fundamental perturbations in the precise relationship between local wind forcing and local radar backscatter variations. What is central for this letter is the acknowledgement that long-wave tilting of these short-scale waves is an additional second-order but fundamental perturbation that can impinge on any assumed direct relation between local wind forcing and radar backscatter variation, particularly at near-nadir incidence angles. A substantial fraction of the longer tilting gravity wave field is due to swell and wind seas generated by distant or turning winds, which are uncoupled and misaligned with the local wind.

Previous investigations have used bulk wave statistical parameters such as significant wave height (SWH) to demonstrate long-wave variability impacts upon σ_0 [15], [22], [23], [29] and more widely on retrieved winds [12], [13], [21], [27], [28]. Such observations have clearly shown long-wave effects on altimeter backscatter and have led to the development of an operational wind speed model for the satellite altimeter that utilizes both σ_0 and SWH [7], [13], where fortuitously both measurements are made from the same platform. SWH is not retrievable using scatterometry.

While altimeter ocean backscatter has been successfully modeled with quasi-specular scattering theory, off-nadir radar backscatter represents a mixture of specular and tilted Bragg resonance diffraction processes as the incidence angle extends away from 0° out toward 10°–15°. The transition between the two scattering regimes depends upon the instrument wavelength and the wind speed and has been proposed to occur near an incidence angle of 10°. A notable observation is that close to this angle a lower sensitivity between σ_0 and wind speed is found [14], [19], [25]. This particular feature has been exploited over the ocean to calibrate airborne and spaceborne precipitation or cloud radars—the objective being to minimize uncertainty due to surface wind variations.

The low, or near-nadir, incidence angle range of $1° \leq \theta \leq 18°$, is currently covered by the precipitation radar (PR) on the Tropical Rainfall Mapping Mission (TRMM) [17], [18]. Though designed specifically for the measurement of precipitation profiles in the atmosphere over both land and ocean,

Manuscript received January 5, 2007; revised March 9, 2007.

N. Tran is with the Space Oceanography Division, Collecte Localisation Satellites, 31520 Ramonville St-Agne, France (e-mail: tran@cls.fr).

B. Chapron is with the Centre de Brest, French Research Institute for Exploration of the Sea (IFREMER), 29280 Plouzané, France.

D. Vandemark is with the Ocean Process Analysis Laboratory, University of New Hampshire, Durham, NH 03824 USA.

Digital Object Identifier 10.1109/LGRS.2007.896329

the PR system also acquires sea surface σ_0 under rain-free conditions. Using wind speed estimates from the TRMM Microwave Imager (TMI), a fully empirical model function was built to relate cross section to wind speed for incidence angles from 0° to 18° [11]. This is the first and only satellite system to provide such angle-resolved scattering near nadir, and the objective here is to further examine these data to help bridge what is known regarding the effects of waves on the altimeter and scatterometer. In this letter, we take the advantage of a large collocated database, which is compiled using PR and both Jason-1 and Environmental Satellite (ENVISAT) altimeters, to extend the description of PR σ_0 in terms of wind speed, significant wave height, and incidence angle through a tabulated model function $\sigma_0(\theta, U, \mathrm{SWH})$. This provides a compact and statistically accurate representation permitting the study of the expected wave tilting impacts on the sea surface scattering at these low incidence angles.

II. Data Sets

A. TRMM PR Cross Section

The TRMM satellite was launched in November 1997 carrying five instruments including the PR. Since the focus of TRMM is to measure rainfall in the tropics, a low inclination non-sun-synchronous orbit was selected to confine the satellite ground track between 35°S and 35°N. The PR is a Ku-band pulsed radar operating at 13.8 GHz and horizontal polarization. σ_0 measurements are collected through the atmospheric column and from the surface. The PR antenna is an electronically scanned phased array that scans a plane normal to the flight direction (cross-track) through the nadir with measurements at 49 beam positions (e.g., the angle bins 1, 25, and 49 correspond to the incidence angles +18°, 0.1°, and −18°, respectively) over a 215-km ground swath. The scan duration is equal to 0.6 s with a surface pixel provided every 4.3 km both along and cross-track [16], [17] for the original orbit height.

The TRMM orbit was raised from 350 to 403 km in August 2001 to increase the duration of the mission. The spatial resolution of the PR is thus degraded slightly, increasing to 5.0 km by 5.0 km. Our data analysis covers the one-year period of 2003. The high quality of the PR surface ocean σ_0 data for this period was confirmed in two recent studies [11], [31]. The data product used herein is TRMM PR standard product 2A21 (ver. 5) from the Goddard Distributed Active Archive Center. These data include normalized radar cross-section measurements, associated quality flags, and a rain/no-rain flag for each incidence angle bin or pixel [18]. Data over land, with any data quality issue, or with rain over the ocean target are all excluded from the composite data set. Further data processing and satellite-to-satellite crossover selection details follow [31] except that for this letter the search was performed over all incidence angles in the PR ground tracks. As shown in the previous study, the density of crossovers increases with latitude due to the combined altimeter–PR orbit characteristics.

B. Wind Speed and Significant Wave Height Data

We use surface wind speed estimates (U) from the surface model analysis provided by the European Centre for Medium-Range Weather Forecast (ECMWF) as a common reference to quantify PR σ_0 wind dependence. SWH data for the study come from the Jason-1 and ENVISAT altimeters. These satellites also provide an estimate of wind speed using altimeter σ_0 measurements, but ECMWF model winds are used for the model functions developed here explicitly because we do not wish to introduce the known sea state impacts that lie within altimeter wind speed data into the present PR results. The potential negative impact of using the model wind products is that these data are extracted and interpolated from six hourly 1° grid data set and that model winds will always disagree with *in situ* measurements to a certain degree. Thus, the model functions to be developed will be slightly impacted, particularly at lightest wind speed, by this interpolation but previous studies (e.g., [13]) have shown that the systematic nature of wave height impacts should still be quite apparent and similar when using the ECMWF model winds and it is this impact that is the main focus of this letter. While one could go another step to gather TRMM/scatterometer/altimeter triplet crossovers to replace ECMWF winds with those from scatterometry, this step dramatically reduces the data set size without dramatically increasing the quality of the result as the agreement between the ECMWF and scatterometer product is high.

Time/space interpolated ECMWF wind speed and standard altimeter SWH estimates are both available in the Geophysical Data Records (GDR) for these two altimeters. The Jason-1 altimetric mission was launched in December 2001 and placed in the same ground track as its predecessor TOPEX/Poseidon. It carries the Poseidon-2 altimeter that was derived from the experimental Poseidon-1 instrument aboard TOPEX/Poseidon. The satellite flies a nonsun-synchronous orbit at an altitude of 1336 km with an inclination of 66°. Detailed description of the mission and the Poseidon-2 instrument are provided, respectively, in [20] and [5]. The ENVISAT altimeter (called Radar Altimeter 2) was launched on March 2002 and is derived from the European Remote Sensing satellite (ERS)-1 and ERS-2 altimeters [2]. The satellite orbit is sun-synchronous at an altitude of 800 km with an inclination of 98.55° allowing measurement closer to the poles than Jason-1. More details can be found in the ENVISAT product handbook [3]. Parameters from both Jason-1 and ENVISAT GDRs over the one-year period of 2003 are used for this letter. Erroneous altimeter estimates are discarded using conventional data quality flagging [3], [24]. Further data filtering follows from the Cal/Val quality assessment that is routinely performed at the Collecte Localisation Satellites [8]. We use only rain-free data. Since the Jason-1 rain flag, which is currently available at the time of this analysis, uses a TOPEX-derived algorithm that was not yet fine-tuned on Jason-1 measurements, a Jason-1 rain flag was calculated using a more recent algorithm [30]. This algorithm shows higher sensitivity to low intensity rainfall as shown using TMI rain estimates [33].

C. Crossover Selection

The criteria used for the collocation between PR and Jason-1 or ENVISAT crossovers are given as follows: time separation within 1 h and spatial separation less than 100 km. The different collocation sets PR/altimeter/ECMWF are limited in latitude to the tropics within ±35° of the equator due to the TRMM

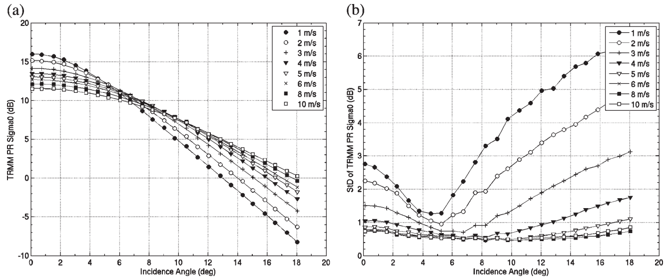

Fig. 1. (a) Mean values and (b) standard deviations of binned PR σ_0 as a function of incidence angle for different wind speeds (SWH between 0.5 and 6.5 m).

orbit. We merge the two data sets using, respectively, Jason-1 and ENVISAT SWH estimates to obtain a unique data set over which the geophysical model function $\sigma_0(\theta, U, \mathrm{SWH})$ can be produced. To insure homogeneity and consistency between altimeter SWH estimates for the two missions, we applied small $[O\ (\mathrm{cm})]$ SWH adjustments per the most recent correction model [26].

III. Near-Nadir Scattering Model

Following the standard quasi-specular backscattering approach, near-nadir σ_0 can be written as

$$\sigma_0(\theta, U, \mathrm{SWH}) = \frac{\rho(U)}{\mathrm{mss}(U, \mathrm{SWH})} \sec^4(\theta) \exp\left[-\frac{\tan^2(\theta)}{\mathrm{mss}(U, \mathrm{SWH})}\right] \quad (1)$$

where σ_0 is the normalized backscatter in natural units (not in decibels), and θ is the incidence angle as previously defined. ρ represents an effective nadir reflection coefficient, and mss is a measure of the effective mean square slope (see [4] for review). The model assumes that sea state dependence of ρ is unlikely or negligible, which is verified to a large extent using the dual frequency capabilities of the TOPEX altimeter [6], [9]. The model also allows for the impact of sea state on the cross section. It is the overall degree of sea state development, which contributes to the mean squared tilting slopes. Yet, the analogy with optical scattering assumption implies that the incident radiation wavelength should be much shorter than all roughness lengths on the surface. For microwave probing of the ocean surface, this is untrue due to the presence of gravity-capillary waves. In particular, at first order and with a Gaussian statistical assumption, the slope variance in (1) corresponds to a filtered slope distribution [35].

As obtained in Fig. 1(a) (see also [11, Fig. 5]), the Gaussian assumption of (1) is qualitatively consistent with the PR data up to about 18°. Observed biases at nadir between altimeter measurements and PR data can be attributed to absolute calibration issues [31]. According to (1), analysis of a single frequency radar altimeter with both wind speed and sea state proxy cannot, with certainty, separate the dependencies related to mss variations from those related to variations of ρ. This is because at nadir, (1) becomes

$$\sigma_0(\theta = 0, U, \mathrm{SWH}) = \frac{\rho(U)}{\mathrm{mss}(U, \mathrm{SWH})}. \quad (2)$$

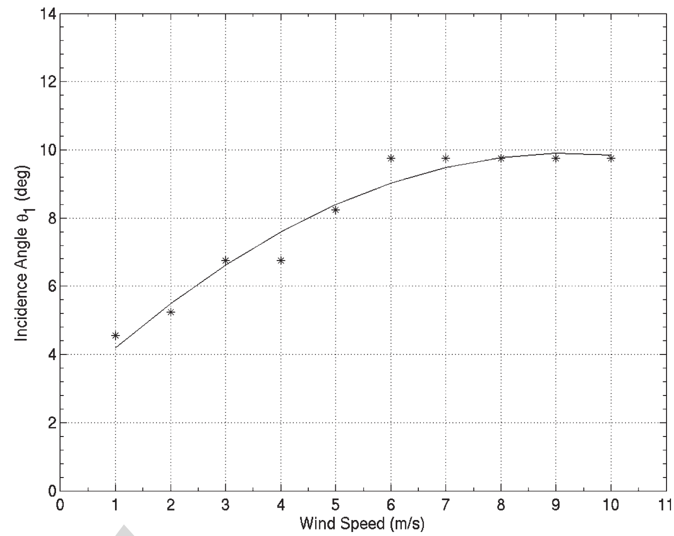

Fig. 2. Incidence angle θ_1 presenting the lowest standard deviation of binned PR σ_0 at a given wind speed as function of wind speed. Overlaid is a quadratic regression fit to better display the trend.

Perhaps more interestingly, the differentiation of (1) with respect to mss yields

$$\frac{\partial \sigma_0}{\partial \mathrm{mss}} = \frac{\tan^2(\theta) - \mathrm{mss}}{\mathrm{mss}^2} \sigma_0. \quad (3)$$

The form of the fractional cross-section variation $(\Delta\sigma_0/\sigma_0)$ in natural units (not in decibels), due to fractional change of mss, will be incidence angle dependent, i.e., 1) when $\tan^2(\theta) <$ mss, $\Delta\sigma_0/\sigma_0 \propto (-\Delta\mathrm{mss}/\mathrm{mss})$ and the nadir viewing altimeter falls in this category, and 2) at higher incidence angles, when $\tan^2(\theta) >$ mss, $\Delta\sigma_0/\sigma_0 \propto (+\Delta\mathrm{mss}/mss)$ and the off-nadir viewing scatterometer falls into this category. The following analysis of the PR σ_0 documents this fractional change of σ_0 with incidence angle.

IV. Analysis of PR Backscatter

A. *Geophysical Model Function for Ku-Band Ocean σ_0 at Low Incidence Angles*

We restrict this letter to light-to-moderate wind speed conditions up to 11 m/s. At wind speeds above this range, complex nonlinear surface wave structure and foam involved with large-scale wave breaking become critical to the surface description and the radar scattering from it. While these higher winds are important, the extensive amount of data that fall at or below 11 m/s and the physics associated with these conditions are the focus of this letter. Two empirical tabular model functions are developed. The first model is based on the analysis of measured σ_0 at each PR incidence angle within specified wind speed intervals and is denoted $\sigma_0(\theta, U)$. The 25 different incidence angles are given as follows: 0.1° (nadir), 0.75°, 1.55°, 2.25°, 3.05°, 3.75°, 4.55°, 5.25°, 6.05°, 6.75°, 7.55°, 8.25°, 9.05°, 9.75°, 10.55°, 11.30°, 12.05°, 12.85°, 13.55°, 14.35°, 15.05°, 15.85°, 16.55°, 17.35°, and 18.05°, and the bin width is about 0.1°. The model is formed from the sample mean σ_0 in each 1-m/s wind speed and incidence angle 2-D bin. A 3σ filter is then applied to eliminate outlier measurements, giving Fig. 1(a). The second model function takes into account both wind speed and significant wave height dependence at each incidence angle. It is denoted as $\sigma_0(\theta, U, \mathrm{SWH})$. The wind speed bin width is still 1 m/s, and the SWH bin width is set to 1 m.

B. $\sigma_0(\theta, U)$

Fig. 1(a) shows that results from nadir to 5° in incidence angle are monotonically decreasing in σ_0 as wind speed increases. Above 10°, σ_0 becomes a monotonically increasing function of wind speed. In the range $5^\circ \le \theta \le 10^\circ$, σ_0 first increases, then decreases with increasing wind speed with a low sensitivity to wind speed. The standard deviations of the σ_0 measurements in each (θ, U) bin are shown in Fig. 1(b) with respect to incidence angle for different wind speeds. For all wind speeds, standard deviations reach a minimum value at an incidence θ_1 between 4° and 10°. Higher magnitudes of standard deviation are associated with light wind speeds, and these magnitudes decrease with increasing wind speed. Magnitudes are smaller at nadir (0.1°) than at 18° for light wind speeds up to 5 m/s. Above 5 m/s, results show similar values. In the range $4^\circ \le \theta \le 10^\circ$, σ_0 not only exhibits low sensitivity to wind speed but also an overall low variability. This lowered variability is related to (3). The angle θ_1, in Fig. 2, roughly identifies the condition $\tan^2(\theta) = \mathrm{mss}(U)$ for which the fractional cross-section variation is minimum, and the shift of θ_1 with wind speed corresponds to the anticipated increase of mss. As found, there is an increase of θ_1 with increasing wind speed up to 7 m/s followed by a saturation trend toward $\sim 10^\circ$ for higher moderate winds.

C. $\sigma_0(\theta, U, SWH)$

The very large collocated data set compiled enables the analysis of the combined incidence angle and SWH dependencies on σ_0 using the narrow 1-m/s wind speed bin. Fig. 3 displays a difference factor δ defined as $[\sigma_0(\theta, U, \mathrm{SWH}) - \sigma_0(\theta, U)]$, in decibels, with respect to incidence angle at four selected wind speeds of 2, 5, 7, and 10 m/s. For all winds, behavior of δ as a function of SWH is clear. At low SWH ($\sim$1 m) representing young sea, δ decreases with increasing angle, whereas for higher SWH ($\sim$4 m associated mostly with mixed seas including swell) δ exhibits the opposite trend. The overall picture shows that at a given wind speed, all curves (linear least-squares fits) associated to the different 1-m SWH classes intersect at a particular value of incidence angle θ_2 that shifts with respect to wind speed value.

Very similar results are obtained when reducing the crossover collocation criteria. A subset is extracted for measurements collocated in time to within 1/2 h and 25 km in space. Fig. 4 is the same as Fig. 3 but only for the case of two moderate wind speeds (7 and 10 m/s) for which there is still sufficient data (minimum of 100 samples per bin) to compute statistically stable indicators.

The relative magnitude of σ_0 for extreme conditions, i.e., low and high SWH (1 and 4 m, respectively), is shown in Fig. 5 as a function of incidence angle for light-to-moderate wind speeds. For all wind speeds, we observe a positive magnitude at low incidence angles that decreases to reach a negative value at higher incidence. At 2-m/s wind, the magnitude is, respectively, $\sim$0.8 dB at nadir and -1.6 dB at $\sim 18^\circ$. At 10 m/s, we observe almost similar absolute magnitude of variation ($\sim$0.8 dB)

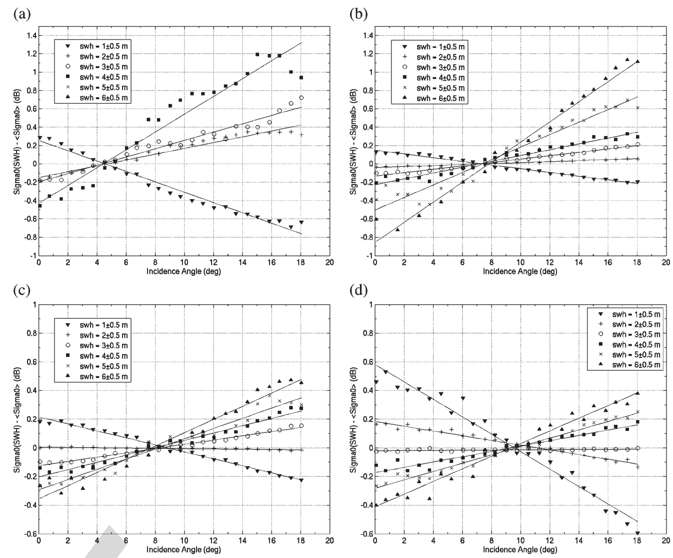

Fig. 3. Difference δ (between averaged PR σ_0 associated to a 1-m class of SWH and the averaged values estimated over all SWH) as function of incidence angles for various SWH classes at selected wind speeds: (a) 2 m/s, (b) 5 m/s, (c) 7 m/s, and (d) 10 m/s (1-m/s bin width). Overlaid are linear regression fits to better display the trends.

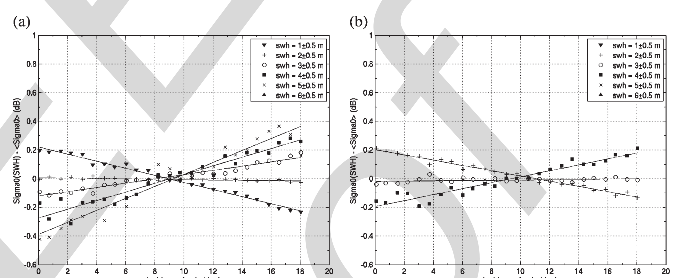

Fig. 4. Same as Fig. 3 but crossover data are selected with narrower selection criteria, 25 km and 30 min, for two selected wind speeds: (a) 7 m/s and (b) 10 m/s (1-m/s bin width).

between the two extreme incidence angles. These results are consistent with the previous analysis at higher incidence angles (20°, 30°, 40°, and 60°) in [23] using NUSCAT–SWADE data. AQ2
However, in cases of moderate winds, these authors concluded that the existence of large waves with high SWH will not have significant impact on the radar backscatter since the observed differences were within the uncertainty of the radar ($\pm$1 dB). The large amount of data available here helps to revise these conclusions. For these wind conditions, the presence of large waves significantly impact σ_0 from nadir to 18° except around a particular incidence angle, denoted θ_2 in Fig. 6, where σ_0 is insensitive to SWH at a given wind speed. As found, θ_1 and θ_2 angles are almost equal and correspond to the condition $\tan^2(\theta_1) = \tan^2(\theta_2) = \mathrm{mss}(U)$. Around these critical angles, the backscatter cross section is insensitive to significant wave height variations at a given wind speed.

One point of note for these TRMM PR data is that they represent horizontally polarized returns. There is a recognized difference in the response of horizontal and vertical polarization returns from the sea surface (cf. [1]). The present results, in terms of overall features, can however be easily transposed to a vertically polarized result. Indeed, continuity between nadir viewing returns (no polarization) and scatterometer off-nadir returns in either one of the polarized states indicates that since

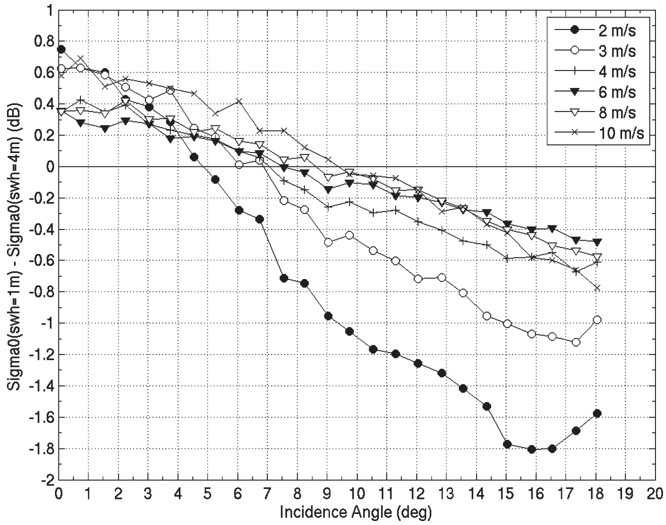

Fig. 5. Magnitude of the difference of σ_0 between low SWH (1 m) and high SWH (4 m) conditions as function of incidence angle for different wind speeds from light to moderate winds.

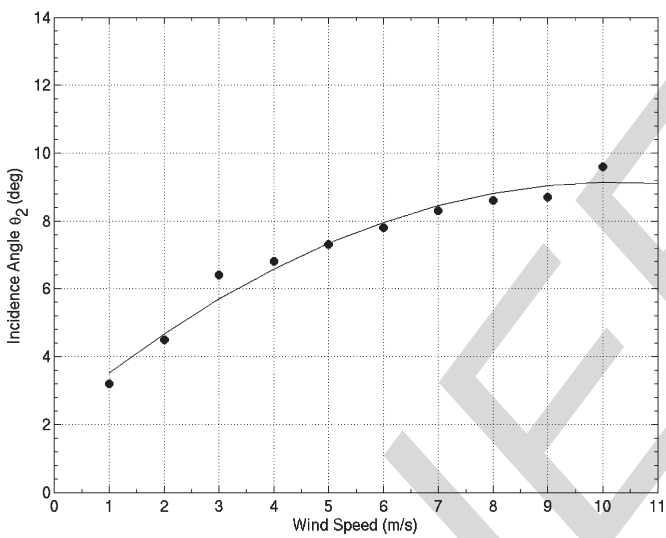

Fig. 6. Incidence angle θ_2 presenting a quasi-insensitivity of PR σ_0 to SWH at a given wind speed as function of wind speed. Overlaid is a quadratic regression fit to better display the trend.

sea state effects are observed in both polarizations when the backscatter is off nadir, all near-nadir measurements will display the same trends (in HH and VV). Previous analysis of the National Aeronautics and Space Administration scatterometer (NSCAT) backscatter in each polarization state shows similar relative sea state impacts with respect to a global averaged backscatter that was derived by mixing all sea state conditions; they are slightly larger for NSCAT HH polarization measurement than on VV polarization data regardless of incidence angles between 16° and 50° [32].

V. Conclusion

New approaches for viewing the global ocean using satellites have become available in the last decade. This letter focuses on sea surface roughness remote sensing and what can be learned using a multiple satellite perspective with the specific goal being to provide new data to bridge the gap between what is known about nadir and off-nadir microwave scattering and emission from the ocean. Near-surface wind speed is a first-order geophysical parameter to be derived from microwave ocean sensors (the scatterometer, radiometer, and altimeter), but it is well known that the transfer function between their raw measurements and wind speed must account for perturbation due to surface wave processes that often deviate from simple local wind forcing behavior. To reduce uncertainties in satellite wind speed retrieval from backscatter measured at different observation angles and to ensure proper assimilation of scatterometer and altimeter data into numerical weather prediction models, it is increasingly apparent that a precise understanding of the relationship between surface roughness through radar backscatter measurement and both wind and wave conditions is very important [28], [29]. Gaining quantitative insight on these sea state perturbations using field studies is notoriously difficult due to the inability to gather the sufficient range of surface conditions and data population.

This letter makes use of a multisatellite ocean observing opportunity, where a new type of ocean surface remote sensing data set, i.e., the TRMM cross-track scanning radar, is combined with coincident sea surface wave height information from crossing satellite altimeters to provide all-new data illustrating wave impacts on radar backscatter at multiple incidence angles. The resulting TRMM PR model function provides results showing that long-wave tilting effects are quantitatively confirmed in line with recent airborne slope measurements [34]. Accordingly, near-nadir cross-section measurements at a given fixed wind speed and ranging in incidence angles out to 20° are measurably related to the sea state dynamics. As a surrogate for the sea state's degree of development, the use of a collocated SWH parameter helps to document this impact and to clearly identify the off-nadir incidence angle that corresponds to the lowest fractional cross-section variation—a very useful angle to know in over-ocean radar calibration activities. For TRMM PR incidence angles that lie closer to scatterometer viewing angles (i.e., 16°–20°), our results show that for light-to-moderate wind conditions the presence of large waves can affect the performance of surface wind retrieval algorithms, which is consistent with previous results (e.g., [27] and [29]). As expected, larger incidence angles are thus certainly to be recommended for surface wind scatterometry to minimize sea state impact. Combined use of both nadir and near-nadir single frequency measurements can also help to infer a sea surface slope variance that can potentially be related to surface wind stress [35] and assimilated into numerical wave models. As obtained, this sea surface slope variance will include both longer wave and shorter wave slope contributions. Dual frequency nadir measurements and/or use of the contemporaneous SWH measurements will then help to remove the longer wave contributions to leave the shorter ones [9]. At nadir and near-nadir configurations, dual frequency capability will thus improve short surface wave observations and surface wind retrieval algorithm performances.

Acknowledgment

The authors would like to thank the Goddard Space Flight Center Distributed Active Archive Center for the straightforward and rapid electronic access to the TRMM PR data. The authors would also like to thank two anonymous reviewers whose comments helped improve the clarity of the document.

REFERENCES

[1] C. Anderson, T. Macklin, C. Gommenginger, M. Srokosz, J. Wolf, and J. Hargreaves, "Impact of sea state on nadir-looking and side-looking microwave backscatter," *Earth Observation Quart.*, no. 67, pp. 5–8, 2000.

[2] J. Benveniste, M. Roca, P. Vincent, G. Levrini, S. Baker, O.-Z. Zanife, and C. Zelli, "The Envisat radar altimetry mission: RA-2, MWR, DORIS and LRR," *ESA Bull.*, vol. 105, pp. 67–76, 2001.

[3] J. Benveniste, S. Baker, O. Bombaci, C. Zeli, P. Venditti, O.-Z. Zanife, B. Soussi, J.-P. Dumont, J. Stum, and M. Pilar Milagro-Perez, *Envisat RA-2/MWR Product Handbook*. Frascati, Italy: Eur. Space Agency, 2002. PO-TN-ESR-RA-0050. [Online]. Available: http://envisat.esa.int/dataproducts/ra2-mwr/CNTR.htm.

[4] G. S. Brown, "Quasi-specular scattering from the air-sea interface," in *Surface Waves and Fluxes*, vol. 2, W. Plant and G. Geerneart, Eds. Norwell, MA: Kluwer, 1990, pp. 1–40.

[5] G. Carayon, N. Steunou, J.-L. Courriere, and P. Thibaut, "Poseidon-2 radar altimeter design and results of in-flight performances," *Mar. Geod.*, vol. 26, no. 3/4, pp. 159–165, Dec. 2003.

[6] B. Chapron, K. Katsaros, T. Elfouhaily, and D. Vandemark, "A note on relationships between sea surface roughness and altimeter backscatter," in *Air-Water Gas Transfer*, B. Jähne and E. C. Monahan, Eds. Hanau, Germany: AEON Verlag & Studio, 1995, pp. 869–878.

[7] F. Collard and S. Labroue, "New wind speed algorithm for Jason-1," presented at the Ocean Surface Topography Science Team Meeting, St. Petersburg, FL, Nov. 2004.

[8] J. Dorandeu, M. Ablain, Y. Faugère, F. Mertz, B. Soussi, and P. Vincent, "Jason-1 global statistical evaluation and performance assessment—Calibration and cross-calibration results," *Mar. Geod.*, vol. 27, no. 3/4, pp. 345–372, 2004.

[9] T. Elfouhaily, D. Vandemark, J. Gourrion, and B. Chapron, "Estimation of wind stress using dual-frequency TOPEX data," *J. Geophys. Res.*, vol. 103, no. C11, pp. 25 101–25 108, 1998.

[10] J. Figa-Saldana, J. J. W. Wilson, E. Attema, R. Gelsthorpe, M. R. Drinkwater, and A. Stoffelen, "The advanced scatterometer (ASCAT) on the meteorological operational (MetOp) platform: A follow on for European wind scatterometers," *Can. J. Remote Sens.*, vol. 28, no. 3, pp. 404–412, 2002.

[11] M. H. Freilich and B. A. Vanhoff, "The relationship between winds, surface roughness, and radar backscatter at low incidence angles from TRMM precipitation radar measurements," *J. Atmos. Ocean. Technol.*, vol. 20, no. 4, pp. 549–562, Apr. 2003.

[12] R. Glazman and A. Greysukh, "Satellite altimeter measurements of surface wind," *J. Geophys. Res.*, vol. 98, no. C2, pp. 2475–2484, Feb. 1993.

[13] J. Gourrion, D. Vandemark, S. Bailey, B. Chapron, C. P. Gommenginger, P. G. Challenor, and M. A. Srokosz, "A two-parameter wind speed algorithm for Ku-band altimeters," *J. Atmos. Ocean. Technol.*, vol. 19, no. 12, pp. 2030–2048, Dec. 2002a.

[14] V. Hesany, W. J. Plant, and W. C. Keller, "The normalized radar cross section of the sea at 10° incidence," *IEEE Trans. Geosci. Remote Sens.*, vol. 38, no. 1, pp. 64–72, Jan. 2000.

[15] W. C. Keller and W. J. Plant, "Cross-sections and modulation transfer functions at L and Ku-bands measured during the tower ocean wave and radar dependence experiment," *J. Geophys. Res.*, vol. 95, no. C9, pp. 16 277–16 289, 1990.

[16] T. Kozu *et al.*, "Development of precipitation radar onboard the tropical rainfall measuring mission (TRMM) satellite," *IEEE Trans. Geosci. Remote Sens.*, vol. 39, no. 1, pp. 102–116, Jan. 2001.

[17] C. Kummerow, W. Barnes, T. Kozu, J. Shiue, and J. Simpson, "The tropical rainfall measuring mission (TRMM) sensor package," *J. Atmos. Ocean. Technol.*, vol. 15, no. 3, pp. 809–817, Jun. 1998.

[18] C. Kummerow *et al.*, "The status of the tropical rainfall measuring mission (TRMM) after two years in orbit," *J. Appl. Meteorol.*, vol. 39, no. 12, pp. 1965–1982, Dec. 2000.

[19] H. Masuko, K. Okamoto, M. Shimada, and S. Niwa, "Measurement of microwave backscattering signatures of the ocean surfaces using X and Ka-band airborne scatterometers," *J. Geophys. Res.*, vol. 91, no. C11, pp. 13 065–13 083, 1986.

[20] Y. Menard, L.-L. Fu, P. Escudier, F. Parisot, J. Perbos, P. Vincent, S. Desai, B. Haines, and G. Kunstmann, "The Jason-1 mission," *Mar. Geod.*, vol. 26, no. 3/4, pp. 131–146, 2003.

[21] F. Monaldo and E. Dobson, "On using significant wave height and radar cross section to improve radar altimeter measurements of wind speed," *J. Geophys. Res.*, vol. 94, no. C9, pp. 12 699–12 701, Sep. 1989.

[22] S. V. Nghiem, F. K. Li, and G. Neumann, "The dependence of ocean backscatter at Ku-band on oceanic and atmospheric parameters," *IEEE Trans. Geosci. Remote Sens.*, vol. 35, no. 3, pp. 581–600, May 1997.

[23] S. V. Nghiem, F. K. Li, S. H. Lou, G. Neumann, R. E. McIntosh, S. C. Carson, J. R. Carswell, E. J. Walsh, M. A. Donelan, and W. M. Drennan, "Observations of ocean radar backscatter at Ku and C-bands in the presence of large waves during the surface wave dynamics experiment," *IEEE Trans. Geosci. Remote Sens.*, vol. 33, no. 3, pp. 708–721, May 1995.

[24] N. Picot, K. Case, S. Desai, and P. Vincent, *AVISO and PODAAC User Handbook IGDR and GDR Jason Products*, 2003. SMM-MU-M5-OP-13184-CN (AVISO), JPL D-21352 (PODAAC). [Online]. Available: www-aviso.cls.fr/documents/ donnees/produits/handbook_ja son.pdf.

[25] W. J. Plant, "Studies of backscattered sea return with a CW, dual-frequency, X-band radar," *IEEE Trans. Antennas Propag.*, vol. AP-25, no. 1, pp. 28–36, Jan. 1977.

[26] P. Queffeulou, "Long-term validation of wave height measurements from altimeters," *Mar. Geod.*, vol. 27, no. 3/4, pp. 495–510, 2004.

[27] P. Queffeulou, B. Chapron, and A. Bentamy, "Comparing Ku-band NSCAT scatterometer and ERS-2 altimeter winds," *IEEE Trans. Geosci. Remote Sens.*, vol. 37, no. 3, pp. 1662–1670, May 1999.

[28] Y. Quilfen, B. Chapron, and D. Vandemark, "On the ERS scatterometer wind measurements accuracy: Evidence of seasonal and regional biases," *J. Atmos. Ocean. Technol.*, vol. 18, pp. 1684–1697, 2001.

[29] Y. Quilfen, B. Chapron, F. Collard, and D. Vandemark, "Relationship between ERS scatterometer measurement and integrated wind and wave parameters," *J. Atmos. Ocean. Technol.*, vol. 21, no. 2, pp. 368–373, Feb. 2004.

[30] J. Tournadre, "Validation of Jason and Envisat altimeter dual-frequency rain flags," *Mar. Geod.*, vol. 27, no. 1/2, pp. 153–169, 2004.

[31] N. Tran, O.-Z. Zanife, B. Chapron, D. Vandemark, and P. Vincent, "Absolute calibration of Jason-1 and Envisat altimeter Ku-band radar cross section from cross-comparison with TRMM precipitation radar measurements," *J. Atmos. Ocean. Technol.*, vol. 22, no. 9, pp. 1389–1402, 2005a.

[32] N. Tran, "Contribution to analysis of NSCAT and ERS-2 scatterometer data by using neural network methodology—Sea state impact on scatterometer returns," Ph.D. dissertation, Univ. Pierre et Marie Curie, Paris, France, 1999.

[33] N. Tran, E. Obligis, and F. Ferreira, "Comparison of two Jason-1 altimeter precipitation detection algorithms with rain estimates from TRMM microwave imager," *J. Atmos. Ocean. Technol.*, vol. 22, no. 6, pp. 782–794, 2005b.

[34] D. Vandemark, B. Chapron, J. Sun, G. H. Crescenti, and H. B. Graber, "Ocean wave slope observations using radar backscatter and laser altimeters," *J. Phys. Oceanogr.*, vol. 34, no. 12, pp. 2825–2842, 2004.

[35] D. Vandemark, J. B. Edson, and B. Chapron, "Altimeter estimation of sea surface wind stress for light to moderate winds," *J. Atmos. Ocean. Technol.*, vol. 14, no. 3, pp. 716–722, Jun. 1997.

AUTHOR QUERIES

AUTHOR PLEASE ANSWER ALL QUERIES

AQ1 = Please provide keywords.
AQ2 = Please provide the expanded form of “NUSCAT-SWADE”.
AQ3 = Please check if the changes made to this sentence are correct. If not, kindly make the necessary adjustments.

Notes: 1) “ESA publications” was deleted in Ref. [2]. Please check.
2) Ref. [10] was uncited anywhere in the text. Please insert where appropriate.

ATTN: If you are paying to have all or some of your figures appear in color in the print issue, it is very important that you fill out and submit a copy of the IEEE Page Charge & Reprint Form along with your proof corrections. This form is available from the same URL where these page proofs were downloaded from. Thank you

END OF ALL QUERIES